Finite Element Analysis and Response Surface Optimization of a T-Shaped Fillet Welded Joint under Transverse Loading

[1]Tikeshwari Sahu, [2]Mr. Yogesh Deshmukh
[1]Research Scholar, [2]Assistant professor,
[1,2]Department of Mechanical Engineering,
[1,2]Bharti Vishwavidyalay, Durg

Abstract- Welded joints remain one of the most critical and failure-prone elements of fabricated structures, yet their design is still governed largely by empirical rules that do not fully capture the influence of weld geometry on the resulting stress and deformation fields. The present study addresses this gap by carrying out a detailed finite element analysis (FEA) of a T-shaped fillet welded joint subjected to transverse loading, followed by a Design of Experiments (DOE) based Response Surface Optimization (RSO) to quantify the sensitivity of structural responses to weld geometry. A three-dimensional CAD model of the T-joint was developed in ANSYS Design Modeler and discretized using a structured hexahedral mesh of 88,336 nodes and 18,360 elements, with mesh refinement at the weld toe and interface where stress concentration is highest. A fixed support was applied at the base plate and a transverse concentrated load was applied on the vertical member, and a linear static structural analysis was performed to obtain total deformation, equivalent (von Mises) stress, shear stress and normal stress fields. The weld height (P1) and weld base (P2), each varying between 4.2274 mm and 5.7726 mm, were selected as design variables for a nine-point central composite DOE, and response surfaces were generated for total deformation (P3), equivalent stress (P4), shear stress (P5) and normal stress (P6). The results show that the maximum total deformation of approximately 0.090 mm occurs at the free end of the vertical plate, while the maximum equivalent stress of 56.064 to 67.671 MPa, shear stress of 3.52 to 4.23 MPa and normal stress of ±20.4 to ±25.3 MPa are concentrated at the weld toe. Local sensitivity analysis reveals that weld height is the dominant geometric parameter, contributing 87 to 92 percent of the variation in deformation, equivalent stress and normal stress, whereas weld base has a comparatively minor influence. The findings provide a quantitative basis for the geometric optimization of fillet welded T-joints and establish a framework that can be extended to fatigue life prediction and thermal-structural coupled analysis of welded structures.

Index Terms: ***Finite Element Analysis; Fillet Weld; T-Joint; ANSYS; Design of Experiments; Response Surface Optimization; Stress Concentration; Weld Toe; Sensitivity Analysis***

I. INTRODUCTION

Welding is one of the most economical, dependable and widely used permanent metal-joining processes across all branches of industry, from small fabrication workshops to aerospace and shipbuilding. In the welding process, two metal parts are joined under appropriate thermophysical conditions of temperature, pressure and metallurgical composition. A major advantage of welded connections over bolted or riveted joints is that they eliminate the need for additional gusset plates, enable direct transfer of stresses between members, and reduce the overall weight of the structure. Among the various weld types, the fillet weld is the most commonly used owing to its economy and adaptability. Fillet welds may be of concave or convex profile; the concave profile provides a smoother transition between the connected parts and reduces stress concentration compared with the convex profile, although it is more susceptible to cracking and shrinkage related defects. Fillet welds can be broadly classified into two categories. End fillet welds, in which the weld axis is perpendicular to the load axis, exhibit minimal ductility but high strength because the stress developed in the weld is comparable to that of the parent weld metal. Side (longitudinal) fillet welds, in which the weld axis is parallel to the load axis, possess higher ductility but the weld strength is limited to approximately half of the weld metal tensile strength.

1.1 Weld Defects

The mechanical performance of a welded joint is strongly influenced by manufacturing defects such as porosity, cracking, internal concavity and lack of penetration. These defects are particularly critical because they act as initiation sites for fatigue cracks. Incomplete penetration generates local stress raisers that, under cyclic loading, can initiate cracks which appear visually as dark, straight lines along the weld interface. Concavity defects are typically caused by entrapped weld pool slag and similarly degrade fatigue performance.

1.2 Weld Theory and Critical Sections

Fillet and butt welds are the two most common weld types used in fabricated joints. Perpendicular members are typically joined using fillet welds, while parallel surfaces are joined using butt welds; chamfering of the parts is often provided to facilitate full-penetration butt welding, as illustrated in Figure 1 and Figure 1.

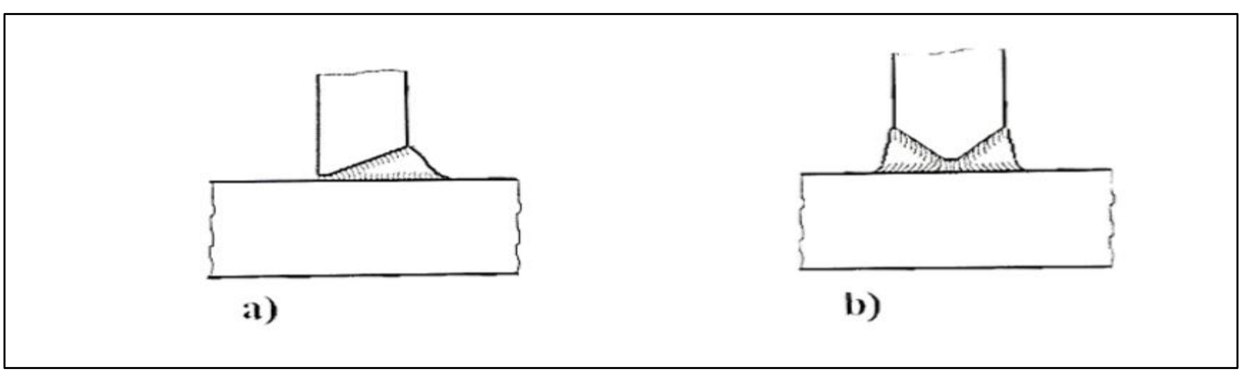

Figure 1: Butt welds in T-joints – (a) single-bevel butt weld, (b) double-bevel butt weld [1]

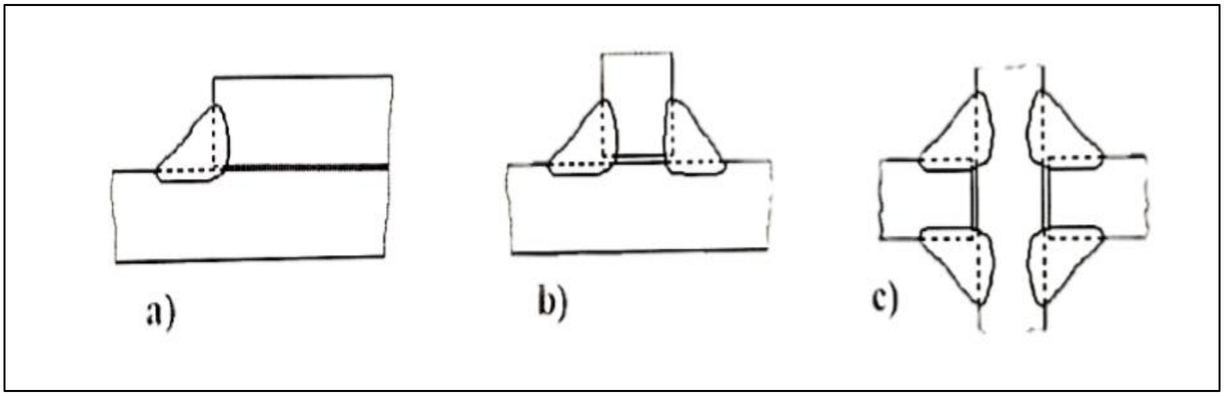

Figure 2: Fillet welds in different joint configurations – (a) lap joint, (b) T-joint, (c) cross joint [1]

From the standpoint of fatigue assessment, the geometry of a fillet weld can be characterized by three critical sections, denoted Section I, Section II and Section III. Crack initiation predominantly occurs in Section III (the weld root), while Section I and Section II correspond to weld-toe crack propagation paths. Correspondingly, three possible failure modes exist in a fillet welded joint: toe cracks at either end of the weld and a root crack at the bottom mid-section of the weld.

II. LITERATURE REVIEW

Nguyen and Wahab [3] investigated misalignments in welded joints and identified eccentricity and angular distortion as the two principal types, noting that the resulting force imbalance can be resolved into axial and bending components that drive fatigue crack initiation and propagation.

Lee [4] employed a fifth-order Runge-Kutta numerical scheme to study large-scale deflections of a cantilever beam incorporating both geometric and material nonlinearity, demonstrating the viability of such numerical methods for assessing fatigue failure of welded joints.

Wilcox [5] reviewed various design approaches for weld joints and highlighted that conventional design methods, which treat fillet weld loading as purely longitudinal, provide only partial results and fail to account for transverse loading effects on weld strength.

Mahapatra et al. [6] experimentally analyzed angular distortion in one-sided fillet welds under constraint conditions and found that properly positioned constraints can counteract welding-induced distortion.

Kumose et al. [7] conducted experimental studies on welded components and observed that higher flange thickness leads to greater free angular distortion, with the amount of distortion strongly dependent on skin stress and pre-straining.

Michaleris et al. [8] showed experimentally that thermal tensioning, which generates tensile strain at the weld toe prior to and during welding, can minimize residual stress and distortion in weld joints.

Okerblom [9] proposed the mismatched thermal strain (MTS) method, an analytical model based on T-joint fillet welds, to determine the curvature induced by welding heat input and demonstrated that the cooling phase produces permanent deformations.

Teng and Lin [10] performed FEA thermal analysis of butt welds to predict transverse residual stresses, comparing results for 10 mm and 15 mm stress-point spacing.

Teng et al. [11] used FEA to predict residual stresses in T-joint fillet welds with stress-point spacing of approximately 3 mm, and found that the restraint condition strongly influences the residual stress generated at the weld toe, decreasing as restraint increases .

Tekriwal and Mazumder [12] used the ABAQUS finite element package to locate residual stresses in butt-welded plates and found that maximum stresses occur in the vicinity of the heat-affected zone (HAZ) boundary, with peak values on both the top and bottom surfaces.

Lassen et al. [13] performed random fatigue life analysis of weld joints and found that the fatigue behaviour at the weld toe does not match the experimental bilinear S-N curve.

Okawa et al. [14] developed a fatigue-life prediction system for welded structures in which small initial cracks at the weld toe are assumed to grow and coalesce, with crack opening/closing behaviour simulated using a strip-yield model that accounts for residual stress and loading sequence effects; the predictions agreed well with actual fatigue tests and the system was shown to be applicable to ships, bridges, plants and construction machinery.

Chattopadhyay et al. [15] performed FEA of weld toes to determine their fatigue characteristics and proposed a peak-stress approach based on classical stress concentration factors that is readily applicable to arbitrary loading combinations.

Acevedo and Nussbaumer [16] investigated residual stresses in bridge tubular joints, finding significant differences between measured (neutron diffraction) and theoretical residual stress values.

Cotrell et al. [17] presented the design, FEA analysis and experimental testing of a two-bladed wind turbine hub, demonstrating adequate strength against fatigue failure of the hub body.

Aygul et al. [18] conducted fatigue-life analysis of an orthotropic bridge deck and characterized three distinct types of weld fatigue failure relevant to bridge, ship and plant structures.

Donders et al. [19] used FEA to study the influence of spot-weld failure on the dynamic performance and robustness of a body-in-white (BIW) automotive structure.

Zhang et al. [20] performed FEA of spot welds in a vehicle chassis under tensile shear loading and found that weld size, sheet thickness and spacing significantly affect the strength of spot-welded joints.

Ertas et al. [21] applied a strain-life approach to FEA fatigue analysis of spot welds and identified the number of spot welds, weld diameter, weld-to-weld spacing and weld-to-edge distance as key parameters governing weld fatigue strength.

Moshayedi et al. [22] performed coupled 2D thermal-mechanical FEA of a weld joint to study nugget formation as a function of welding temperature.

Nacy et al. [23] performed modal vibration analysis of a stiffened conical shell to study the effect of spot welds on natural frequencies, damping factor and mass distribution.

Prasad et al. [24] used Hypermesh-based FEA vibration analysis of spot-welded stiffener plates and validated the predicted natural frequencies against FFT-based experimental results, showing that stiffener profile and pattern are important parameters.

Rusinski et al. [25] studied spot welds under compressive loading including geometric and material nonlinearity, finding that spot-weld pitch and nonlinear effects significantly influence both strength and fatigue life.

Palmonella et al. [26] examined CWELD and ACM2 spot-weld idealizations with respect to natural frequencies and proposed modelling guidelines for body-in-white automotive structures, noting their strong influence on overall structural dynamics.

III. PROBLEM IDENTIFICATION AND OBJECTIVES

3.1 Research Gap

A substantial body of research has examined the operational parameters of welding, such as current, voltage and filler material composition, as well as the mechanisms of fatigue failure, including crack initiation and propagation in welded joints. However, the strength of a fillet welded joint also depends strongly on geometric parameters such as weld size, weld width, throat thickness and weld leg lengths. The individual and combined influence of these geometric variables on key structural responses total deformation, equivalent (von Mises) stress, shear stress and normal stress has not been systematically investigated. This represents a clear gap that motivates the present study.

3.2 Objectives

1. To develop a three-dimensional CAD model and a refined finite element mesh of a T-shaped fillet welded joint in ANSYS Workbench.
2. To perform a linear static structural analysis of the T-joint under transverse loading and evaluate the total deformation, equivalent (von Mises) stress, shear stress and normal stress fields, with particular attention to the weld toe region.
3. To identify weld height and weld base as design variables and construct a Design of Experiments (DOE) to systematically vary these parameters.
4. To generate response surfaces relating weld geometry to the structural responses and to validate the response surface model against the FEA results.

5. To perform a local sensitivity analysis to quantify the relative influence of weld height and weld base on each structural response, and to identify an optimal design region that minimizes deformation and stress concentration.

IV. METHODOLOGY

The methodology adopted in this study follows the standard FEA workflow of pre-processing (CAD modelling and meshing), solution (application of loads, boundary conditions and solver settings), and post-processing (extraction of result fields), followed by a Design of Experiments based Response Surface Optimization to study the effect of weld geometry on structural performance.

4.1 CAD Modelling

A three-dimensional CAD model of the T-shaped fillet weld joint was developed in the ANSYS Design Modeler using sketch and extrude operations. The model consists of a horizontal base plate and a vertical plate joined by a triangular fillet weld bead along the junction, as shown in Figure 3.

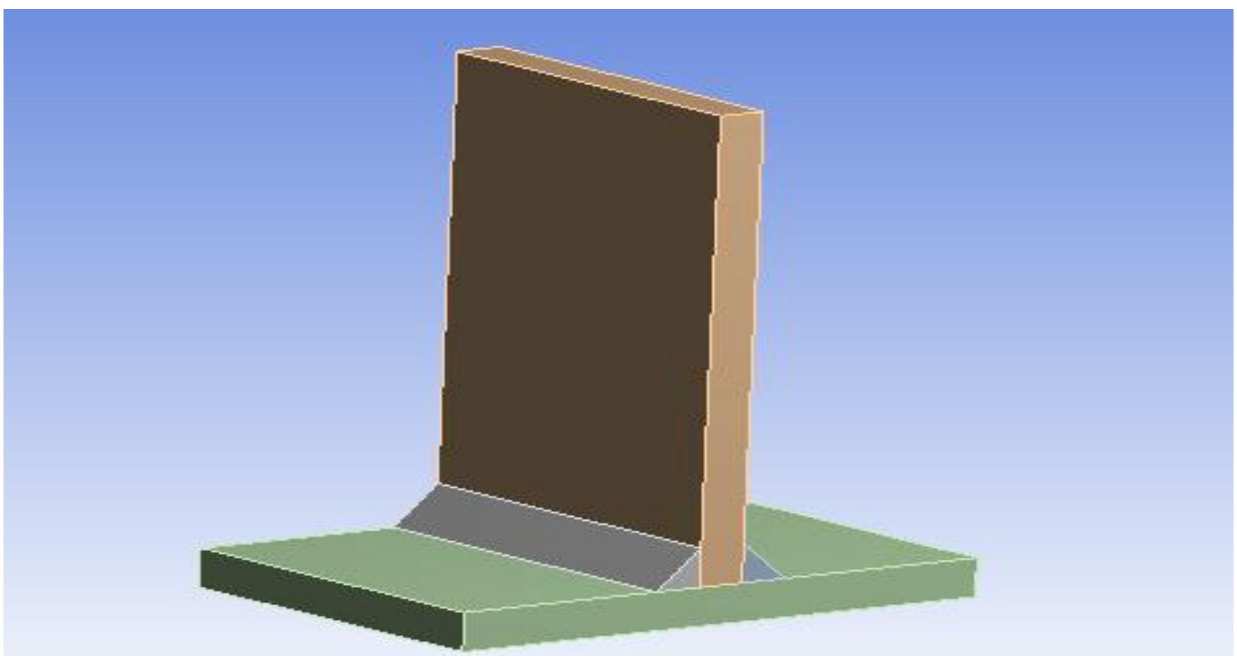

Figure 3: Three-dimensional CAD model of the T-shaped fillet weld joint

Two geometric features of the weld bead, denoted H2 (weld base) and V1/V3 (weld height), were defined as parameters within ANSYS Design Modeler. These two dimensions were subsequently selected as the input design variables for the Design of Experiments and Response Surface Optimization study, since they directly govern the effective throat thickness and load-transfer characteristics of the weld.

4.2 Meshing

The finite element discretization of the T-shaped weld joint was performed using a structured meshing approach in ANSYS Mechanical to obtain an optimal balance between computational efficiency and solution accuracy. A hexahedral (brick) element formulation was adopted owing to its superior capability for capturing stress gradients and minimizing numerical error compared with tetrahedral elements. The geometry was partitioned to facilitate mapped meshing, producing a uniform, well-aligned mesh across both the vertical and horizontal members. A relatively finer mesh was applied at the weld toe and weld interface, where the highest stress concentrations were anticipated, while a coarser mesh was retained in less sensitive regions to reduce computational cost (Figure 4).

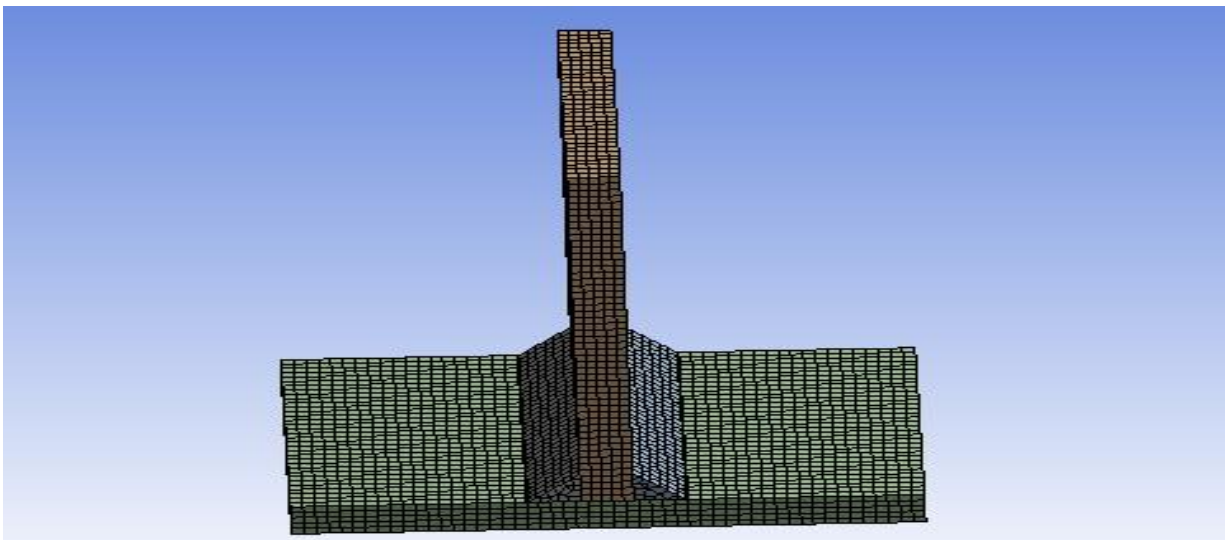

Figure 4: Hexahedral mesh of the T-shaped weld joint, with refinement at the weld toe and interface

The final mesh comprised a total of 88,336 nodes and 18,360 elements (Table 4.1), representing a sufficiently refined discretization for structural analysis. Element quality metricsaspect ratio, skewness and orthogonality were maintained within acceptable limits to ensure numerical stability and convergence.

Table 1: Mesh setting

Mesh Parameter	Value
Element type	Hexahedral (brick), 8-node
Number of nodes	88,336
Number of elements	18,360
Meshing approach	Structured / mapped mesh
Mesh refinement zone	Weld toe and weld interface

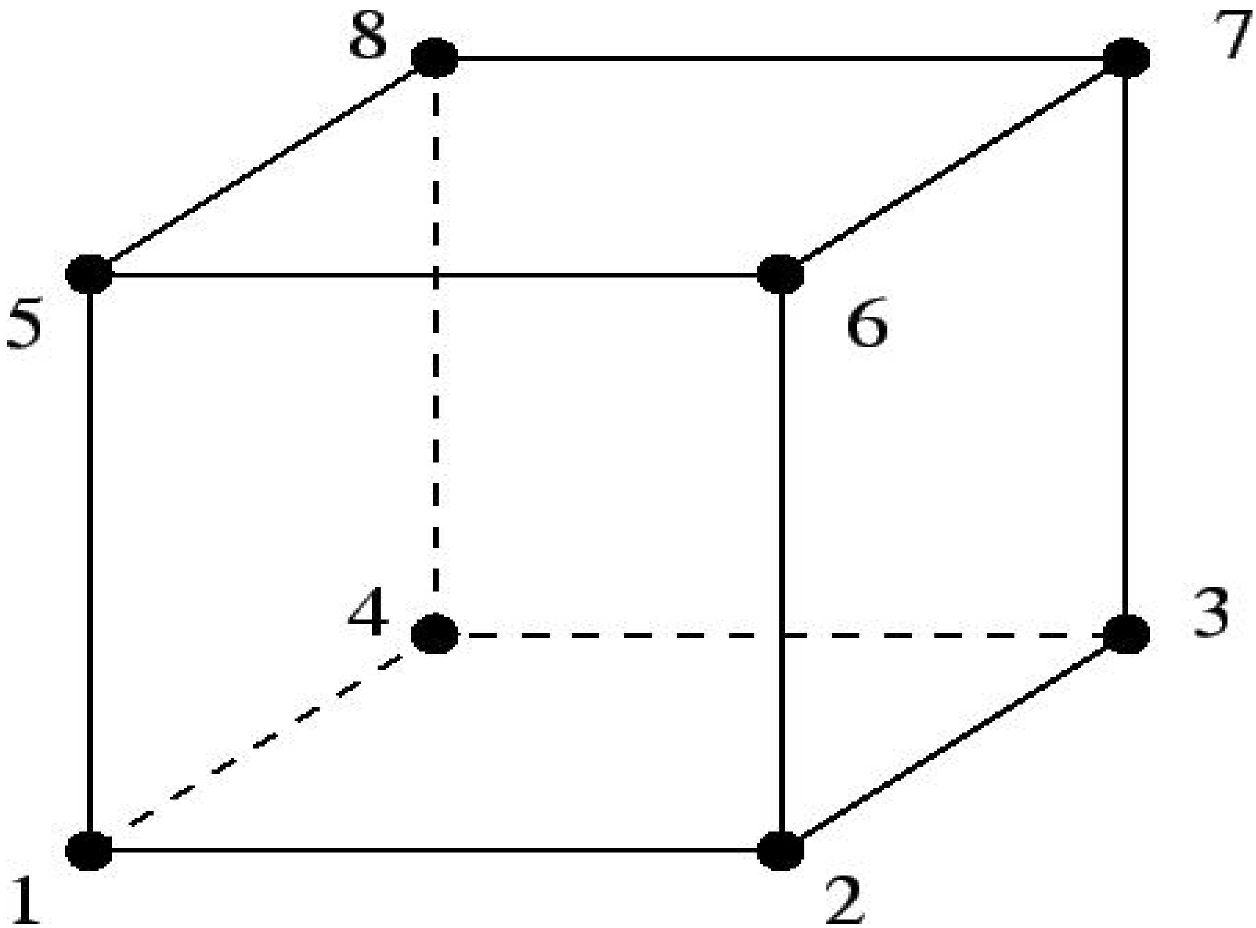

Figure 5: Eight-noded hexahedral (brick) finite element with three translational degrees of freedom per node, defined by six quadrilateral faces, twelve edges and eight corner nodes

The interpolation of field variables such as displacement within the hexahedral element is performed using trilinear shape functions, which ensure continuous variation of displacement across the element domain and an accurate representation of linear strain distribution. Compared with tetrahedral elements, the hexahedral formulation exhibits better convergence characteristics, lower numerical stiffness and improved accuracy in regions of high stress gradient such as weld joints, while also allowing efficient mesh generation with good control over element quality.

4.3 Loads and Boundary Conditions

The base plate of the T-shaped weld joint was constrained using a fixed support, restricting all translational and rotational degrees of freedom at the bottom surface and providing a stable foundation for the analysis. A transverse concentrated force was applied on the vertical plate, directed horizontally and perpendicular to the vertical member, as illustrated in Figure 6. This loading configuration is representative of practical scenarios in which welded T-joints are subjected to transverse forces, generating a combination of bending moment, shear force and localized stress concentration at the weld interface and weld toe.

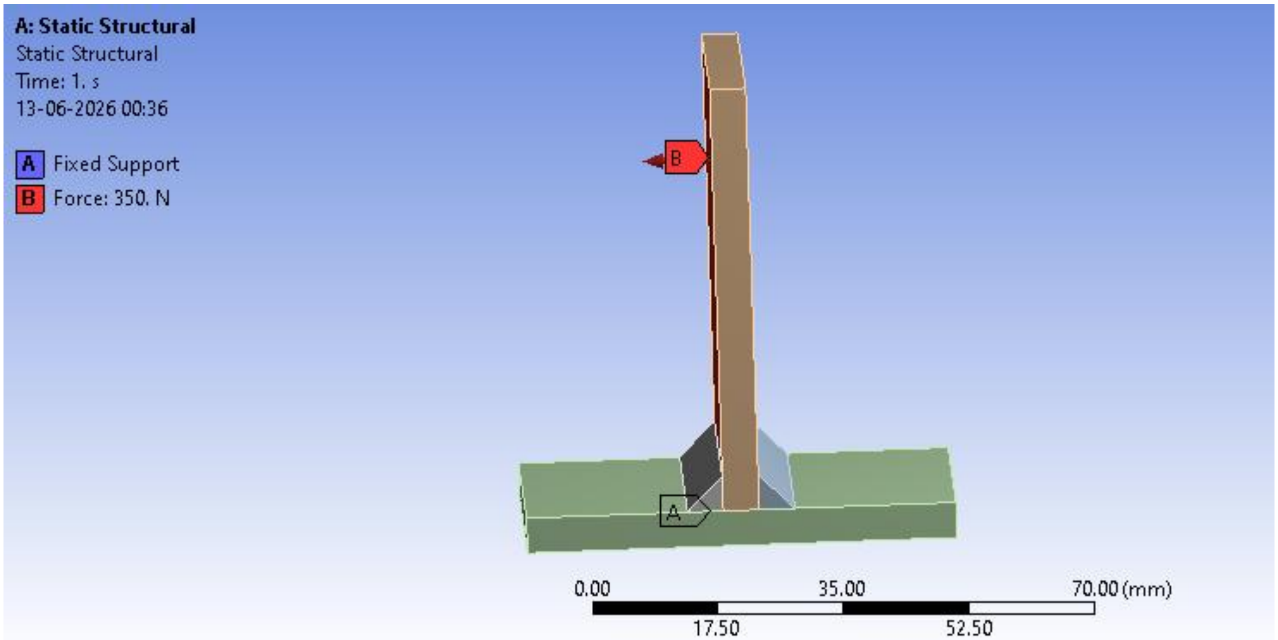

Figure 6: Boundary conditions – fixed support applied at the base plate (region A) and transverse concentrated load applied on the vertical plate (region B)

Table 2: Loads and boundary condition details

Parameter	Value / Description
Support condition	Fixed support at base plate (all DOF = 0)
Applied load	Transverse concentrated force on vertical plate
Load direction	Horizontal, perpendicular to vertical member
Resulting load effects	Bending moment + shear force + stress concentration at weld toe

4.4 Solution Stage

The solution stage was executed using the static structural solver in ANSYS Mechanical, configured to capture the linear elastic response of the T-shaped welded joint. The analysis type was defined as static, assuming time-independent loading with no inertial or damping effects; the total analysis time of 1 second was used purely as a load-step parameter, since the problem is quasi-static. The solver assumed elastic, homogeneous and isotropic material behaviour, and large deformation effects were neglected since the expected deformations lie within the small-strain regime. Solution controls were set to program-controlled settings, allowing ANSYS to automatically select appropriate numerical methods. The global system of equations was solved using a direct sparse solver, well suited for structural problems with a large number of degrees of freedom, ensuring accurate displacement calculation and robust convergence. Since the analysis is linear, convergence was achieved in a single iteration, with internal checks ensuring solution consistency and numerical stability. The output controls were configured to compute and store total deformation, equivalent (von Mises) stress, shear stress and normal stress at the nodal and elemental level, providing the data required to identify critical stress regions, particularly at the weld toe and weld interface.

4.5 Design of Experiments and Response Surface Optimization

In the subsequent stage of the analysis, design variables were selected for performing Response Surface Optimization (RSO) to evaluate the influence of weld geometry on structural performance. Two primary parameters were identified: weld height (P1) and weld base (P2), corresponding to the vertical and horizontal dimensions of the idealized triangular weld cross-section, respectively. These parameters directly determine the effective throat thickness and load-transfer characteristics of the weld joint. Both variables were assigned a baseline value of 5 mm and were varied between 4.2274 mm and 5.7726 mm within ANSYS Workbench using a face-centred Design of Experiments comprising nine design points. Each design point corresponds to an independent finite element simulation, with the resulting output responses total deformation (P3), equivalent stress (P4), shear stress (P5) and normal stress (P6) recorded for subsequent response surface modelling. The selection of weld height and weld base as optimization variables is justified by their strong influence on the mechanical responses, and the response surface methodology enables the relationship between these inputs and the output responses to be established, allowing the identification of optimal weld dimensions that enhance structural performance while minimizing stress concentration.

V. THEORETICAL FORMULATION

The finite element stiffness formulation underlying the static structural solution is based on the principle of minimum total potential energy. Considering a single linear spring of stiffness k subjected to an external force F, with resulting deformation Δ, the work done by the force is given by:

$$W = \Delta \cdot F = \Delta x \cdot Fx = u \cdot F \qquad \text{(Eq. 1)}$$

The strain energy stored in the spring is $U = (1/2)\ K\ \Delta x^2$, and the total potential energy of the loaded spring is therefore:

$$\Pi = (1/2)\ K\ \Delta x^2 - \Delta x \cdot Fx \qquad \text{(Eq. 2)}$$

The equilibrium equation is obtained by minimizing the total potential energy with respect to the unknown displacement Δ, which yields the well-known equilibrium relation:

$$K\ \Delta x = F \qquad \text{(Eq. 3)}$$

For an element with two nodes, each of which may be fixed or free, the same minimization procedure is applied subject to the displacement boundary conditions, with the nodal displacement and force vectors written as $\{\Delta\}^t = [\Delta 1, \Delta 2]$ and $\{F\}^t = [F1, F2]$ respectively. Assembling these element-level stiffness relations for all elements in the mesh yields the global system of equations $[K]\{\Delta\} = \{F\}$, which is solved by the direct sparse solver to obtain the nodal displacement field, from which the deformation, stress and strain results presented in Section 6 are subsequently derived.

VI. RESULTS AND DISCUSSION

6.1 Structural Response of the T-Shaped Weld Joint

The linear static structural analysis was carried out under the boundary conditions described in Section 4.3, and the resulting total deformation, equivalent (von Mises) stress, shear stress and normal stress fields are presented.

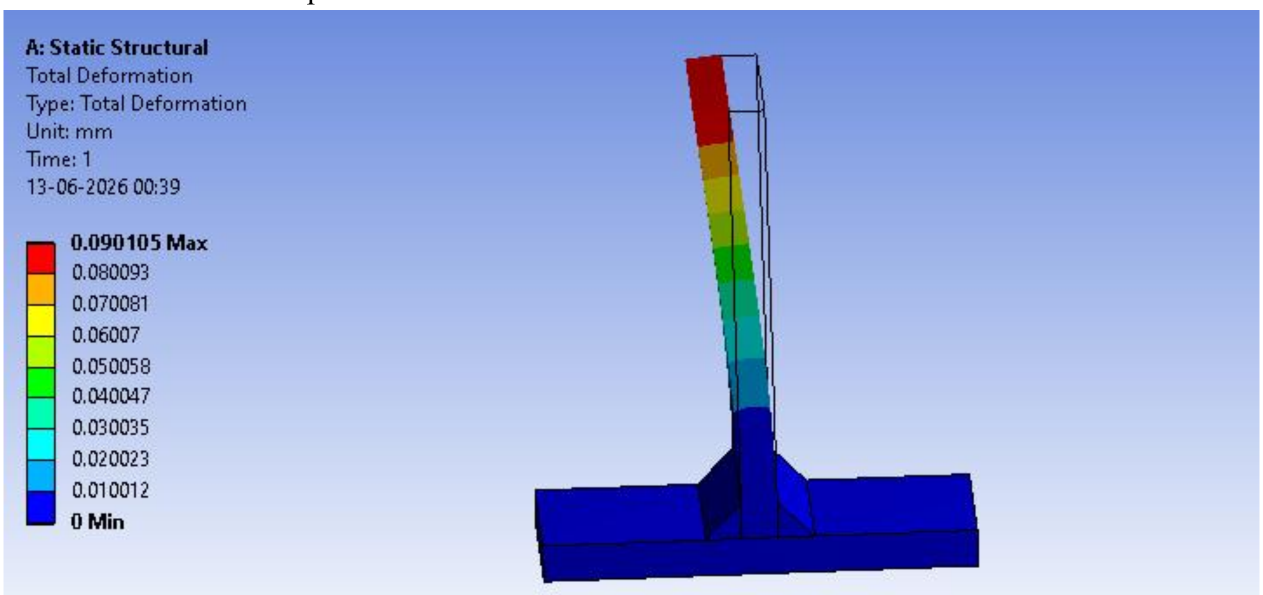

Figure 7: Total deformation contour plot of the T-shaped weld joint

The total deformation plot illustrates the displacement distribution across the T-shaped welded joint under the applied transverse load, with blue indicating minimum deformation and red indicating maximum deformation. The maximum total deformation of approximately 0.090105 mm occurs at the top free end of the vertical plate, consistent with the cantilever-like structural configuration in which the fixed base restricts displacement while the free end experiences the greatest deflection. The deformation decreases smoothly and gradually from the top of the vertical member towards the base, with the minimum deformation of 0 mm observed at the fixed support, confirming correct application of the boundary conditions. The weld region itself, particularly near the joint interface, exhibits relatively low deformation, indicating adequate stiffness in transferring load between the vertical and horizontal members. The smooth, linear deformation gradient along the height of the vertical plate and the absence of abrupt discontinuities indicate elastic behaviour within the applied load range and confirm a well-refined mesh and a stable, converged numerical solution.

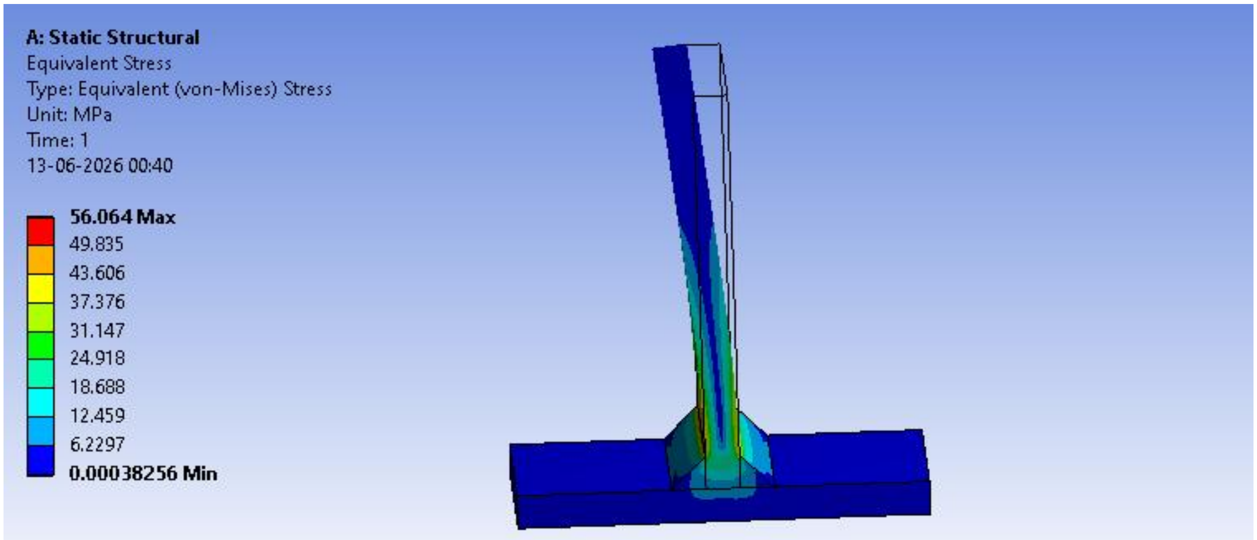

Figure 8: Equivalent (von Mises) stress contour plot of the T-shaped weld joint

The equivalent (von Mises) stress plot shows the maximum equivalent stress of approximately 56.064 MPa highly localized at the weld toe region, near the junction of the vertical and horizontal plates. This concentration is expected due to the abrupt geometric discontinuity and the associated load transfer between the two members, making the weld toe the most critical region for potential failure and a strong candidate location for fatigue crack initiation under cyclic loading. Moving away from the weld interface, the stress magnitude decreases gradually along the height of the vertical plate, transitioning from red and yellow to green and blue regions, while the base plate experiences relatively low stress levels, confirming that the applied load is primarily transferred through the weld region into the support. The minimum stress value of approximately 0.00038 MPa occurs far from the load application point and weld interface, and the smooth stress gradient across the structure indicates a stable, converged solution free of numerical irregularities.

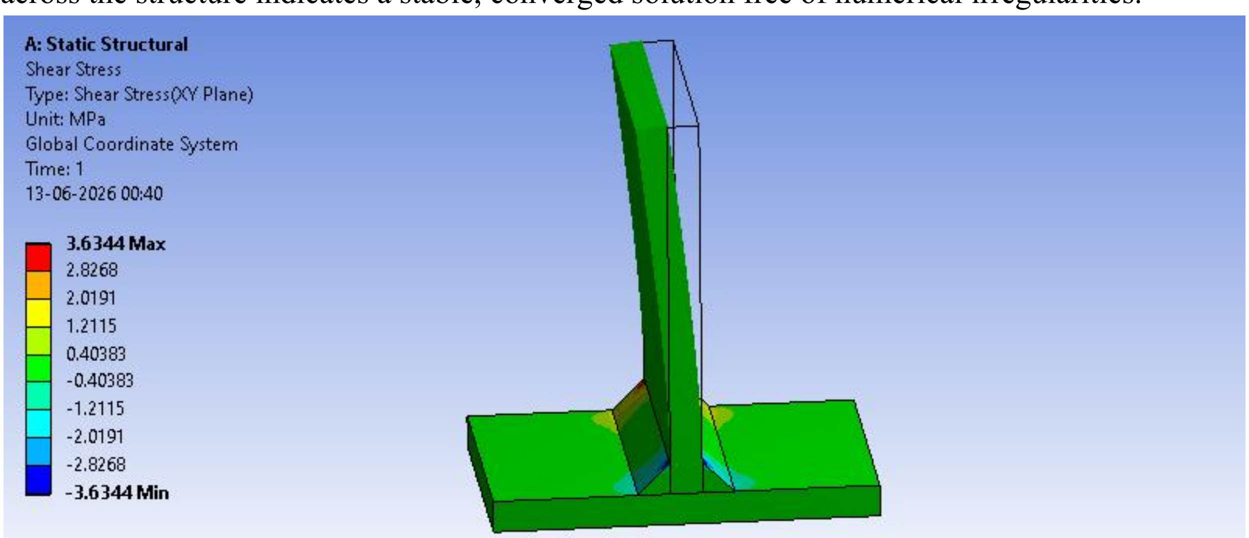

Figure 9: Shear stress (XY-plane component) contour plot of the T-shaped weld joint

The shear stress contour plot, presented for the XY-plane shear stress component, shows both positive and negative shear stress regions, with red indicating maximum positive shear stress, dark blue indicating maximum negative shear stress, and green corresponding to near-zero shear stress. The maximum shear stress of approximately +3.6344 MPa and minimum of −3.6344 MPa indicate a symmetric distribution of shear stress within the structure. The highest magnitude of shear stress is concentrated in the weld region at the junction of the vertical and horizontal plates, particularly near the weld toe, as the applied transverse load generates significant shear forces transferred through the weld interface. The close proximity of positive and negative shear stress zones reflects a stress-reversal phenomenon characteristic of bending-dominated loading, while away from the weld interface the structure predominantly exhibits low (near-zero) shear stress, confirming that the majority of shear load transfer occurs at the joint.

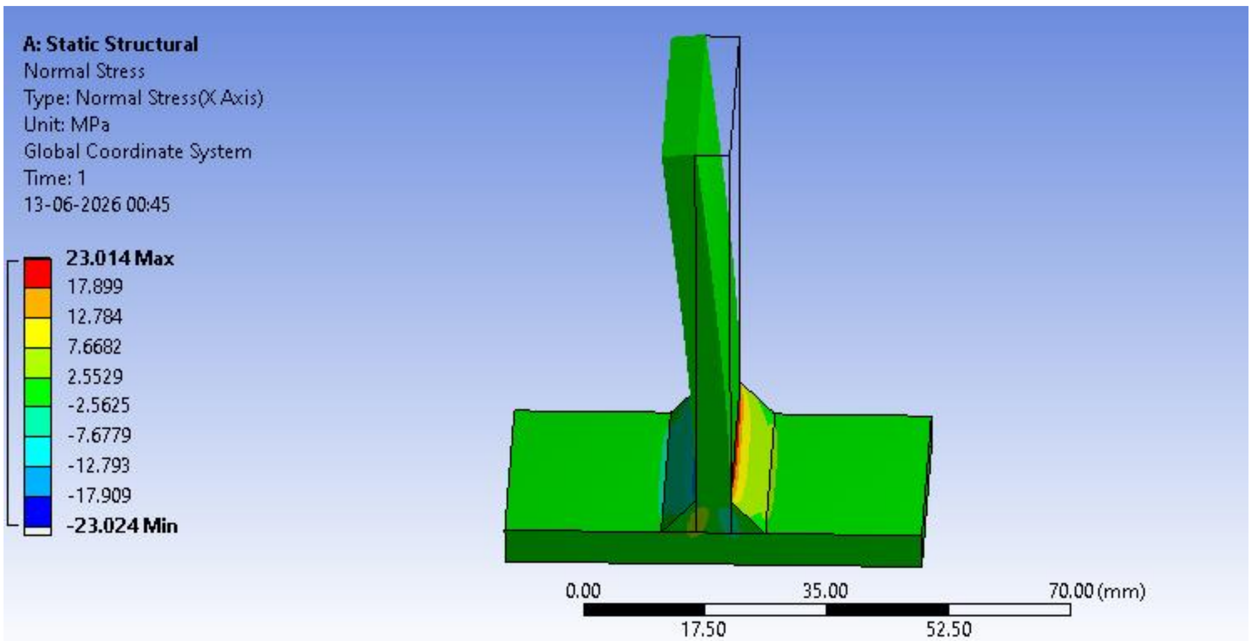

Figure 10: Normal stress (X-direction component) contour plot of the T-shaped weld joint

The normal stress contour plot, presented for the X-direction component, shows both tensile and compressive stress regions, with red indicating maximum tensile stress and dark blue indicating maximum compressive stress. The maximum normal stress is approximately +23.014 MPa (tensile) and the minimum is approximately −23.024 MPa (compressive), with both peak values concentrated at the weld interface and weld toe region due to bending effects induced by the transverse load — one side of the weld experiences tension while the opposite side experiences compression. The clear gradient from tensile to compressive stress across the weld region is characteristic of bending-dominated structures, where the neutral axis separates the tensile and compressive zones, highlighting the critical nature of the weld toe under repeated loading. Away from the weld interface, both the vertical and horizontal plates exhibit relatively low normal stress, confirming that the majority of load transfer and stress concentration is localized within the weld zone.

6.2 Design of Experiments

To systematically evaluate the influence of weld geometry on structural performance, a Design of Experiments (DOE) approach was employed using ANSYS Workbench, with weld height (P1) and weld base (P2) as input design variables, each varied between approximately 4.2274 mm and 5.7726 mm about a baseline of 5 mm. The DOE table consists of nine design points, each corresponding to an independent finite element simulation, with the resulting output responses recorded in Table 3.

Table 3: Design of experiments table

DP	P1 - Weld Height (mm)	P2 - Weld Base (mm)	P3 - Total Deformation (mm)	P4 - Equivalent Stress (MPa)	P5 - Shear Stress (MPa)	P6 - Normal Stress (MPa)
1	5.0000	5.0000	0.090105	56.0640	3.6344	23.0140
2	4.2274	5.0000	0.092040	62.3740	3.9400	25.1110
3	5.7726	5.0000	0.087861	67.6710	3.5211	20.8620
4	5.0000	4.2274	0.090427	60.1820	3.6553	23.3600
5	5.0000	5.7726	0.089895	60.1110	3.9014	22.7710
6	4.2274	4.2274	0.092233	61.4940	3.7284	25.2970
7	5.7726	4.2274	0.088349	66.5300	3.5539	21.4050
8	4.2274	5.7726	0.091926	62.6150	4.2296	24.9940
9	5.7726	5.7726	0.087506	66.8060	3.5858	20.4490

The results show that total deformation varies only within a narrow band (approximately 0.0875 to 0.0922 mm), indicating relatively stable deformation behaviour across the design space. In contrast, the equivalent (von Mises) stress shows a much wider variation, ranging from approximately 56.064 to 67.671 MPa, indicating that the stress response is highly sensitive to changes in weld geometry. Similarly, the shear stress ranges from approximately 3.52 to 4.23 MPa, and the normal stress ranges from approximately 20.449 to 25.297 MPa, indicating moderate sensitivity to the input variables. A comparative review of the DOE table reveals that lower weld height and base combinations tend to increase stress values (indicating reduced stiffness), higher weld dimensions generally produce lower deformation and more favourable stress distributions (although the relationship is not strictly linear), and certain intermediate combinations exhibit optimized responses, highlighting the need for multi-variable optimization through response surface modelling.

6.3 Statistical Distribution of Design Variables

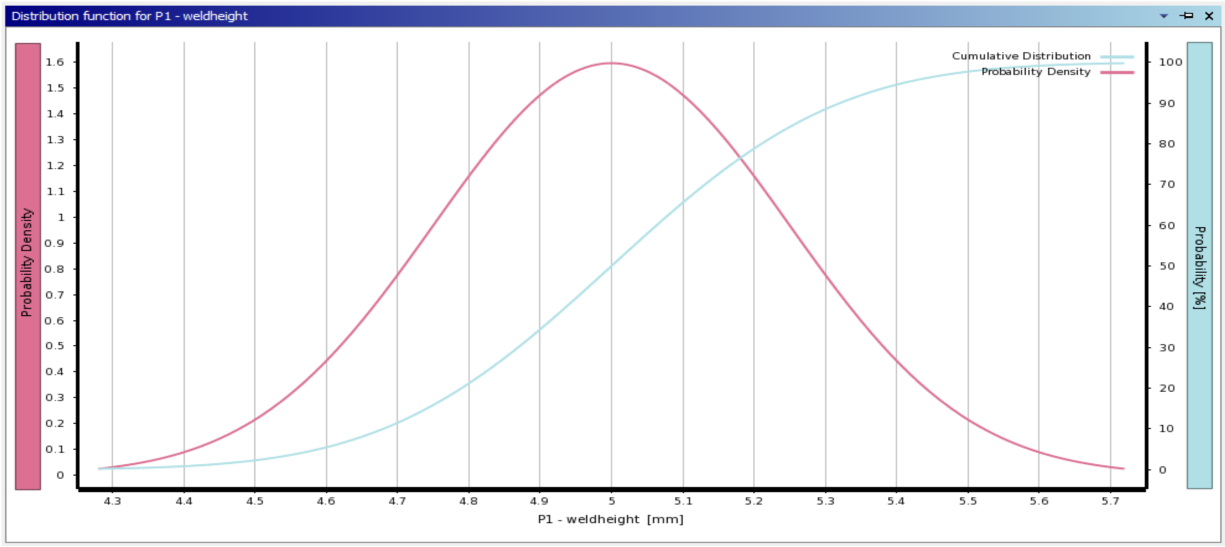

Figure 11: Probability density function (red) and cumulative distribution function (blue) of weld height (P1) used in the DOE

Figure 11 shows the probability density function (PDF, red curve) and cumulative distribution function (CDF, blue curve) of the input design variable weld height (P1). The PDF follows a normal (Gaussian) distribution centred on the mean value of approximately 5 mm, with decreasing probability toward the lower and upper bounds of approximately 4.3 mm and 5.7 mm; the bell-shaped curve indicates that most design points are concentrated near the central value, as is typical of DOE-based parametric studies. The CDF follows the corresponding S-shaped (sigmoidal) curve, rising from 0% probability at the minimum value to 100% at the maximum value, with approximately 50% cumulative probability at the mean. The symmetry of both curves confirms an unbiased exploration of the design space, with the spread reflecting the variation of approximately ±0.7 mm considered in the DOE.

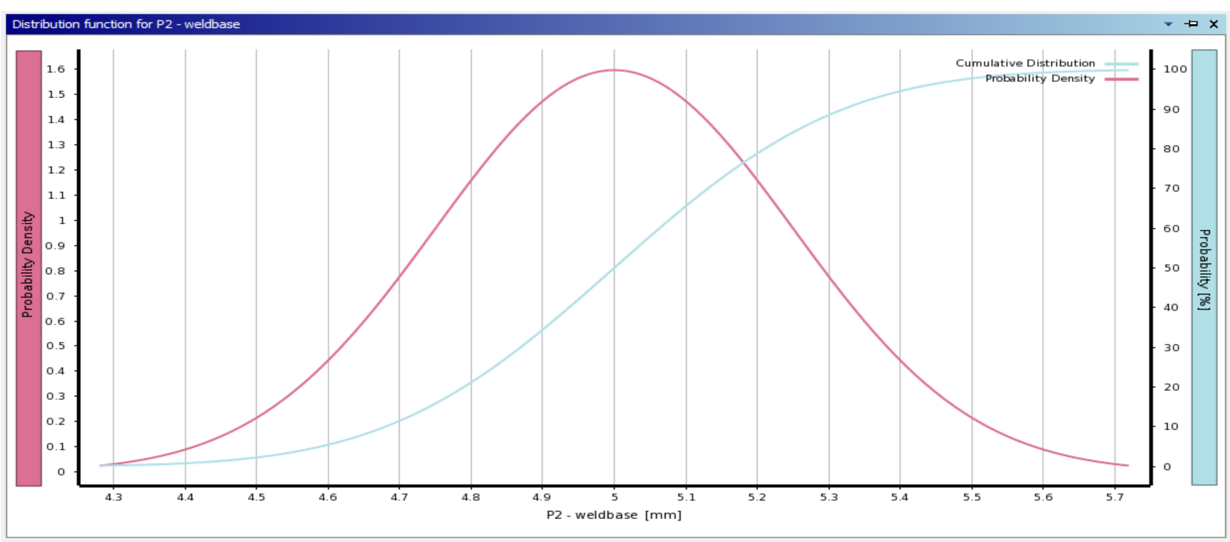

Figure 12: Probability density function (red) and cumulative distribution function (blue) of weld base (P2) used in the DOE

Figure 12 presents the analogous PDF and CDF for the weld base (P2). As with weld height, the PDF follows a normal distribution centred at approximately 5 mm with the design points concentrated near the mean and decreasing symmetrically toward the bounds of approximately 4.3 mm to 5.7 mm, while the CDF follows the corresponding S-shaped curve with the midpoint corresponding to the mean value. The smooth, continuous and symmetric nature of both curves confirms a well-defined probabilistic model for weld base, ensuring that this parameter is varied systematically and statistically across its range and thereby enabling accurate modelling of its influence on the output responses, as well as supporting subsequent sensitivity analysis and identification of optimal design regions.

6.4 Response Surface Model Validation

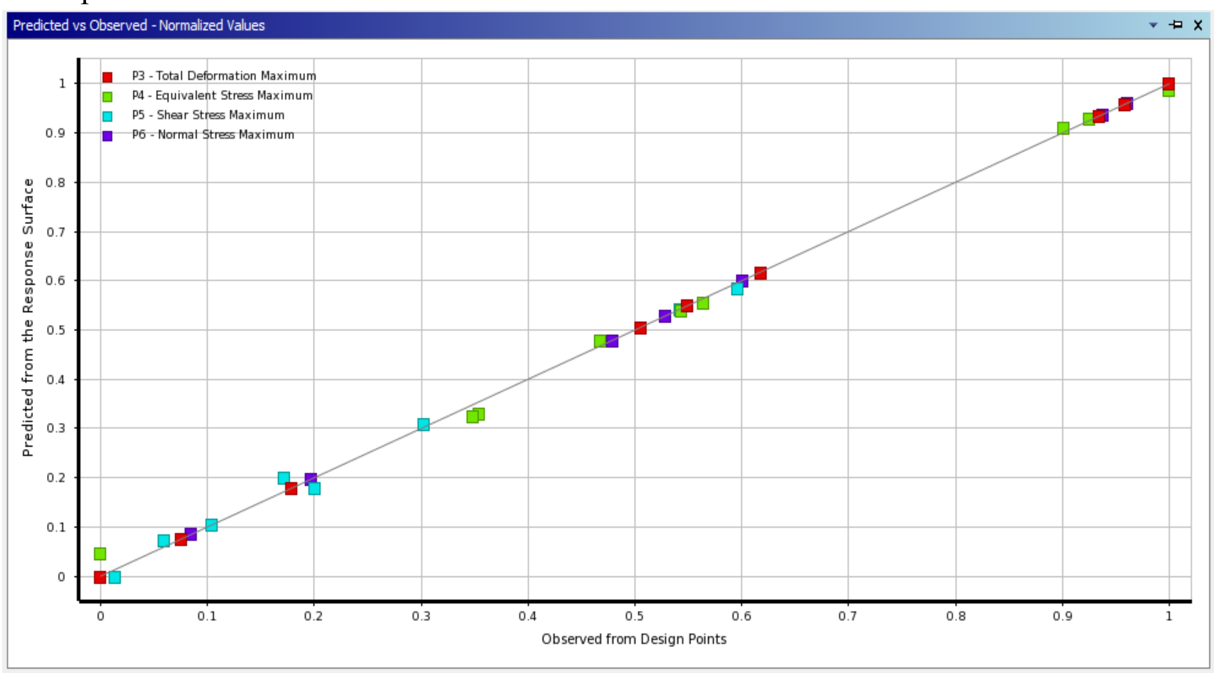

Figure 13: Comparison of predicted (response surface model) versus observed (FEA) normalized values for total deformation (P3), equivalent stress (P4), shear stress (P5) and normal stress (P6)

Figure 13 compares the predicted values obtained from the response surface model against the observed values from the corresponding FEA design points, for all four response parameters total deformation (P3), equivalent stress (P4), shear stress (P5) and normal stress (P6) represented by different coloured markers. The horizontal axis represents the observed (FEA) values and the vertical axis represents the predicted (response surface) values, with the diagonal 45-degree reference line indicating the condition of perfect agreement. The data points for all four response parameters lie closely along the diagonal line, confirming a strong agreement between predicted and actual values and demonstrating the high accuracy and reliability of the developed response surface model in capturing the relationship between the input variables (weld height and weld base) and the output structural responses.

6.5 Effect of Weld Geometry on Total Deformation

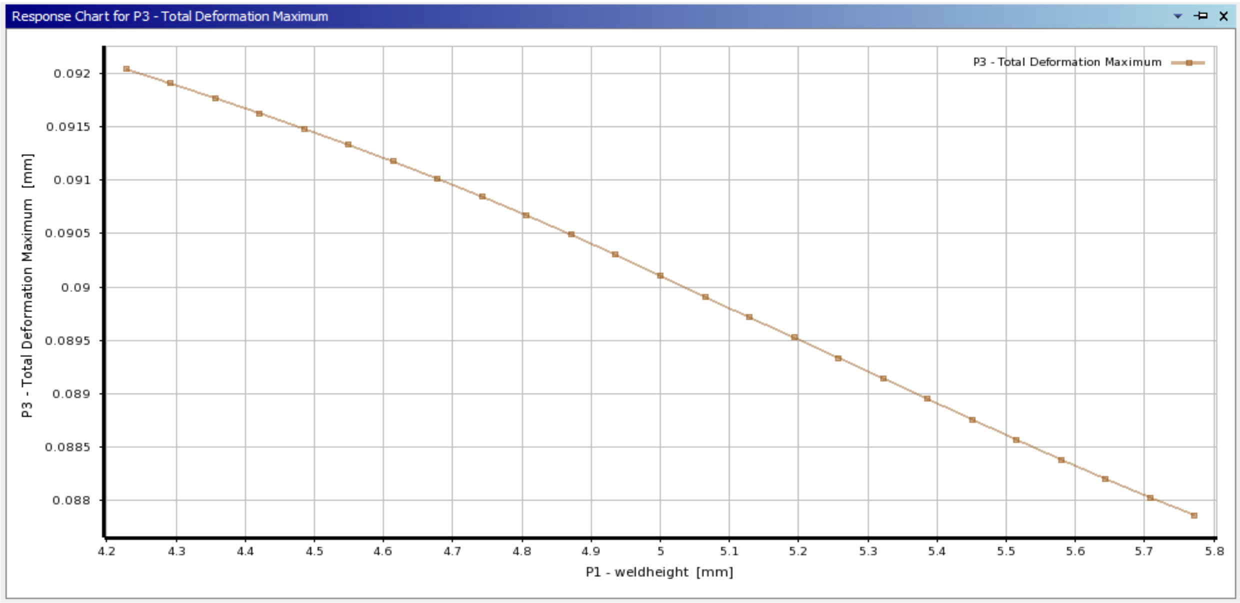

Figure 14: Response surface trend of total deformation (P3) versus weld height (P1)

Figure 14 shows the relationship between weld height (P1) and total deformation (P3) obtained from the response surface model. A clear inverse relationship is observed: as weld height increases from approximately 4.2 mm to 5.8 mm, the total deformation decreases from about 0.092 mm to 0.088 mm, in a smooth and nearly linear trend with no fluctuations or irregularities, confirming the stability and accuracy of the response surface model. Physically, a higher weld height increases the effective throat thickness, improving load-transfer capability and increasing resistance to bending and deflection, thereby reducing the overall deformation of the structure. This demonstrates that weld height is a critical parameter influencing deformation, and increasing its value contributes positively toward enhancing structural rigidity.

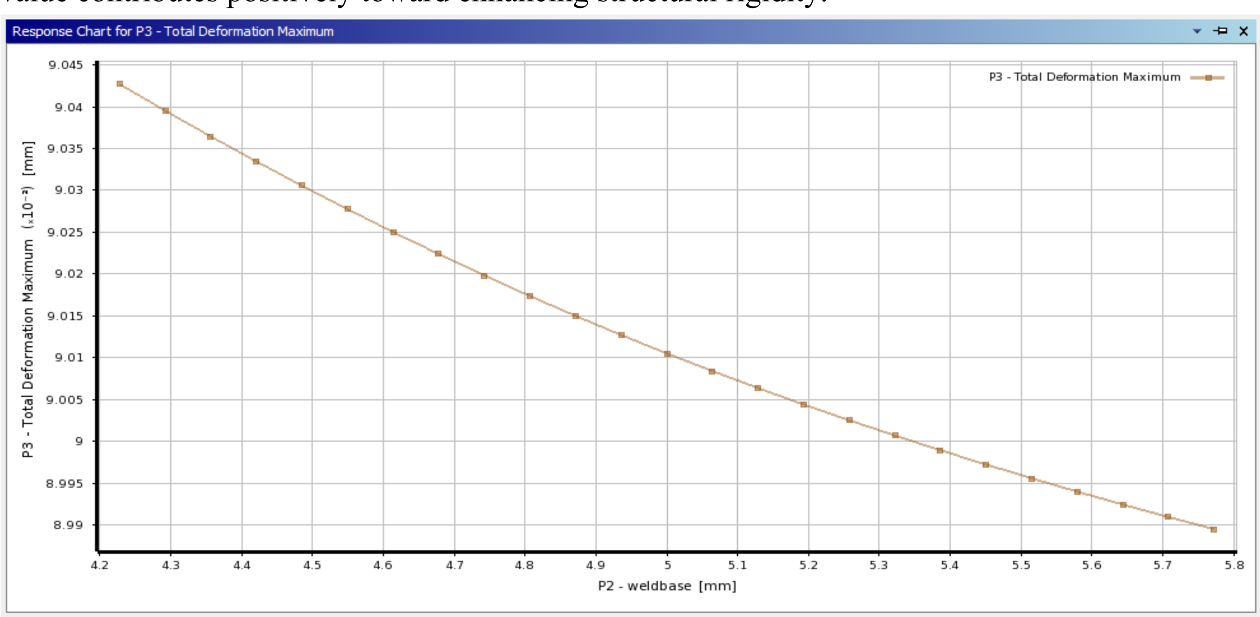

Figure 15: Response surface trend of total deformation (P3) versus weld base (P2)

Figure 15 shows the corresponding relationship between weld base (P2) and total deformation (P3). A gradual decreasing trend in total deformation is observed with increasing weld base, with deformation values varying within a narrow range of approximately 9.045×10^{-2} mm to 8.99×10^{-2} mm as weld base increases from 4.2 mm to 5.8 mm, indicating that the influence of weld base on deformation is relatively moderate compared with weld height. The curve exhibits a smooth, nearly linear downward trend, confirming a stable and consistent relationship and a well-fitted response surface model. Physically, increasing the weld base enhances the load-distribution area at the joint interface and improves the stability and rigidity of the connection, resulting in slightly reduced deformation under the same loading conditions; however, compared with weld height, the effect of weld base is less pronounced, confirming weld height as the dominant parameter influencing deformation behaviour.

VII. CONCLUSION AND FUTURE SCOPE

7.1 Conclusion

Based on the complete finite element analysis, DOE study, response surface modelling and sensitivity analysis of the T-shaped welded joint, the following conclusions are drawn:

- The finite element analysis successfully captured the structural behaviour of the welded joint under transverse loading, validating the suitability of ANSYS for weld analysis.
- The deformation pattern confirms cantilever-type behaviour, with maximum displacement occurring at the free end of the vertical plate.
- The maximum total deformation observed is approximately 0.090 mm, which lies within acceptable limits for structural performance.
- The equivalent (von Mises) stress is highly concentrated at the weld toe region, identifying it as the most critical location for failure initiation.
- The maximum equivalent stress is approximately 56–67 MPa depending on weld geometry, indicating strong sensitivity to design parameters.
- Shear stress distribution shows both positive and negative regions near the weld interface, confirming the presence of bending and load transfer effects, with maximum magnitude approximately 3.5–4.2 MPa localized at the weld junction.
- Normal stress analysis reveals both tensile and compressive stresses at the weld region due to bending, with values ranging from approximately ±20.4 to ±25.3 MPa.
- Weld geometry significantly influences all response parameters, confirming the importance of geometric optimization in welded joint design.
- From the DOE analysis, total deformation shows relatively small variation, while the stress parameters exhibit higher sensitivity to changes in weld dimensions.
- Response surface plots indicate that increasing weld height and weld base generally reduces deformation and stress, improving structural performance.

- Weld height is identified as the most dominant parameter influencing deformation, equivalent stress, shear stress and normal stress, contributing approximately 88–92% influence on deformation and stress responses, while weld base has comparatively minor influence (typically below 35%).
- An optimal design region exists where moderate-to-high weld height combined with an appropriate weld base minimizes stress concentration and deformation.
- The response surface methodology and DOE approach proved effective in predicting structural responses and can be reliably used for optimization of welded joint geometry.

7.2 Future Scope

Based on the outcomes of the present study, several potential areas for future research are identified to further enhance the understanding and performance of welded structures:

- The present study is limited to static structural analysis; future work can incorporate fatigue life analysis using S–N curves or fracture mechanics approaches to predict crack initiation and propagation in welded joints.
- Thermal-structural coupled analysis can be conducted to account for welding heat input, residual stresses and thermal distortions, which significantly influence weld performance.
- Residual stress modelling using advanced welding simulation techniques, such as moving heat source models, can provide more realistic results.
- Dynamic and vibration analysis, including modal analysis and harmonic response, can be performed to evaluate the behaviour of welded joints under cyclic and dynamic loading.
- The effect of torsional loading and multi-axial stress states on weld joints can be investigated to simulate real-world loading scenarios.
- More complex geometries, such as multi-pass welds, multi-joint assemblies and real structural components, can be analyzed to extend applicability.
- The study can be extended by incorporating material nonlinearity, plastic deformation and large deformation effects for more accurate representation under high loads.
- The influence of different materials and weld filler compositions on structural performance can be evaluated.
- Advanced optimization techniques, such as genetic algorithms, particle swarm optimization or machine learning based optimization, can be applied for improved design solutions.
- The integration of probabilistic analysis and uncertainty quantification can be performed to account for variability in material properties and manufacturing defects.

REFERENCES

[1] Olsson, C. (2005). Konstruktions handbok för svetsade produkter, 3rd ed. Lidingö: Industrilitteratur.

[2] Olsson, C. (2014). Konstruktions handbok för svetsade produkter, 5th ed. Onsala: Techstrat Publishing.

[3] T. N. Nguyen and M. A. Wahab, "The effect of weld geometry and residual stresses on the fatigue of welded joints under combined loading."

[4] Kyungwoo Lee, "Large deflections of cantilever beams of nonlinear elastic material under a combined loading," International Journal of Non-Linear Mechanics, 37 (2002) 439–443.

[5] Robb C. Wilcox, "The effect of weld penetration on tensile strength of fillet welded joints," B.S., Naval Architecture and Marine Engineering, U.S. Coast Guard Academy, 1991.

[6] Mahapatra, M., G. L. Datta, B. Pradhan, and N. R. Mandal, "Modelling the effects of constraints and single axis welding process parameters on angular distortions in one-side fillet welds," Proc. IMechE, 221 Part B: 397–407.

[7] Kumose, T., T. Yoshida, T. Abbe, and H. Onoue, "Prediction of Angular Distortion Caused by One-Pass Fillet Welding," Welding Journal, 1954: 945–956.

[8] Michaleris, P., J. Dantiz, and D. Tortorelli, "Minimization of welding residual stress and distortion in large structures," Welding Journal, 11 (1999): 361–366.

[9] Okerblom, N. O., "The Calculations of Deformations of Welded Metal Structures," 1958, Her Majesty's Stationery Office, London.

[10] Teng, T., and C. Lin, "Effect of welding conditions on residual stresses due to butt welds," International Journal of Pressure Vessels and Piping, 75 (1998): 857–864.

[11] Teng, T., C. Fung, P. Chang, and W. Yang, "Analysis of Residual Stresses and Distortions in T-Joint Fillet Welds," International Journal of Pressure Vessels and Piping, 78 (2001): 523–538.

[12] Tekriwal, P., and J. Mazumder, "Transient and Residual Thermal Strain-Stress Analysis of GMAW," Journal of Engineering Materials and Technology, 113 (1991): 336–343.

[13] Lassen, T., Ph. Darcis, and N. Recho, "Fatigue behaviour of welded joints, part 1 – Statistical methods for fatigue life prediction," supplement to the Welding Journal, American Welding Society and Welding Research Council, 2005, pp. 183–187.

[14] Okawa, T. et al., "A fatigue life prediction system for welded structures based on fatigue crack growth simulation considering residual stress and loading sequence."

[15] Chattopadhyay, A. et al., "FEA-based analysis of weld toe fatigue characteristics using classical stress concentration factors."

[16] Acevedo, C., and A. Nussbaumer, "Residual stress assessment of welded bridge tubular joints by neutron diffraction."

[17] Cotrell, J. et al., "Design, analysis and testing of a two-bladed hub."

[18] Aygul, Mustafa et al., "Fatigue life analysis of orthotropic bridge decks - types of weld fatigue failure."

[19] Donders, S. et al., "Effect of spot weld failure on dynamic vehicle Body-In-White (BIW) structural performance."

[20] Zhang, X. et al., "FEA investigation of spot welds on vehicle chassis under tensile shear loads."

[21] Ertas, A. H. et al., "FEA fatigue life analysis of spot welds using the strain-life approach."

[22] Moshayedi, H. et al., "2D FEA thermal analysis of weld joints for nugget formation prediction."

[23] Nacy, S. M. et al., "Vibrational (modal) analysis of a stiffened conical shell with respect to spot weld effects."

[24] Prasad, K. et al., "FEA vibration analysis of spot-welded stiffener plates using Hypermesh."

[25] Rusinski, E. et al., "FEA analysis of spot welds under compressive loads considering geometric and material nonlinearities."

[26] Palmonella, M. et al., "Studies on CWELD and ACM2 spot weld idealizations with respect to natural frequencies in automotive bodies."